NASA Technical Memorandum 100061

Wave Drag and High-Speed Performance of Supersonic STOVL Fighter Configurations

Donald A. Durston and Ronald K. Stonum

January 1988

NASA
National Aeronautics and
Space Administration

NASA Technical Memorandum 100061

Wave Drag and High-Speed Performance of Supersonic STOVL Fighter Configurations

Donald A. Durston, Ames Research Center, Moffett Field, California
Ronald K. Stonum, U. S. Air Force, Moffett Field, California

January 1988

National Aeronautics and
Space Administration

Ames Research Center
Moffett Field, California 94035

A supersonic STOVL fighter aircraft aerodynamic research program is being conducted at NASA Ames Research Center. The research focuses on technology development for this type of aircraft and includes generating an extensive aerodynamic database and resolving particular aerodynamic uncertainties for various twin- and single-engine aircraft concepts. Highlights of the results from this program are presented. The highlights include propulsion-induced effects on the aircraft drag, prediction capabilities, volume integration for minimizing drag, and wave drag and aerodynamic efficiency comparisons. Results indicate that estimated STOVL fighter performance is roughly comparable to the performance of modern conventional fighters in terms of wave drag and aerodynamic efficiency.

SUPERSONIC FIGHTER AIRCRAFT DEVELOPMENT with vertical or short takeoff and landing (V/STOL) capability *and* performance comparable to conventional fighter aircraft has proved to be a formidable challenge over the years. The primary reason for the challenge is that the propulsion system of a V/STOL fighter is usually heavier and occupies more internal volume than the propulsion system of a comparable conventional takeoff and landing (CTOL) fighter. The V/STOL propulsion system is more complicated because it requires the additional ducts, valves, nozzles, and burners necessary to direct the thrust downward and balance the aircraft in engine-borne flight. The additional drag due to the extra weight of the propulsion system hinders the V/STOL fighter's speed and turning performance. Also the extra internal volume occupied by the V/STOL propulsion system limits the V/STOL aircraft range and payload capability relative to CTOL fighters. The need to balance the thrust in hovering flight often dictates that the engine be located at or near the center of the airplane. This central location can degrade the aircraft performance by distorting the cross-sectional area distribution and causing higher wave drag. The nozzles also may be located where they could create problems with scrubbing drag and excessive heating and vibration of the structure in the vicinity of the plume. The plume expanding in proximity to the fuselage may cause additional wave drag as well. Reference 1 discusses these propulsion-system related problems in detail regarding the development of high-speed VTOL and V/STOL fighter aircraft.

Aerodynamic technology studies for supersonic V/STOL and STOVL (short takeoff and vertical landing) fighter aircraft in the U.S. have been addressing the performance trade-off's resulting from their unique propulsion systems. (The acronyms V/STOL and STOVL are sometimes used interchangeably, but STOVL is more accurate for the concepts discussed herein because of preferred operational modes.) The most promising of these propulsion systems are represented in a series of twin- and single-engine supersonic STOVL fighter aircraft concepts being studied at NASA Ames Research Center. This paper presents selected highlights pertaining to high-speed aerodynamic technology development for supersonic STOVL fighter aircraft. These highlights include considerations of airframe/propulsion integration, aerodynamic prediction capabilities, and integration of propulsion systems and other components in the aircraft. In addition, wave drag and aerodynamic efficiency comparisons will be made for various STOVL and CTOL fighters. The aerodynamics relating to the takeoff, transition, and landing flight modes of STOVL fighters will not be discussed in this paper, but are given extensive treatment in other papers for the conference.

STOVL FIGHTER AIRCRAFT CONCEPTS

The Aerodynamics Division of NASA Ames began a series of studies in 1977 to develop the aerodynamic technology for supersonic STOVL fighter aircraft. Under joint NASA/Navy sponsorship, airframe contractors were asked to define realistic STOVL fighter concepts, perform preliminary aerodynamic analyses, identify aerodynamic uncertainties associated with their concept(s), and propose a wind tunnel and analytical research program to resolve as many of the uncertainties as possible. A total of five twin-engine (Fig. 1) and four single-engine (Fig. 2) concepts were investigated in these studies (2–4).*

The propulsion systems used in the nine concepts shown in these two figures represent a broad cross-section of those systems which are the most promising in powered lift technology today. Ejectors are used in the twin-engine General Dynamics E-205 (5), and in the single-engine General Dynamics E-7 (6) and Rockwell concepts (7). A remote augmentor lift system (RALS) is used in the twin-engine General Dynamics R-104 (5) (see later figure), Grumman 623 (8), and Northrop HATOL (9) (horizontal attitude takeoff and landing) concepts. Vectored thrust is used in the single-engine McDonnell Douglas 279-3 (10) concept, while a tandem fan is used in the single-engine Vought TF-120 (11) concept. The twin-engine Northrop VATOL (12) (vertical attitude takeoff and landing) and Vought VATOL (13) concepts are tail-sitters.

Aerodynamic uncertainties can have a major impact on the success of a particular concept. The uncertainties are defined as the aerodynamic characteristics which cannot be confidently predicted using analytical or theoretical methods alone. Typical uncertainties pertinent to the scope of this paper include the minimum drag variation with Mach number, the supersonic wave drag increment due to the propulsion system installation, the interaction of the propulsive flows with the airframe aerodynamics, and the efficient integration of various aircraft components around the propulsion system. Complete listings of the aerodynamic uncertainties for all of the STOVL fighter concepts in the present study can be obtained in Ref. 2–13.

Test programs were conducted in the Ames Aerodynamics Division wind tunnels for three of the twin-engine concepts and two of the single-engine concepts. The tests have provided a means of resolving many of the identified aerodynamic uncertainties, and they have produced an

* Numbers in parentheses designate references at end of paper.

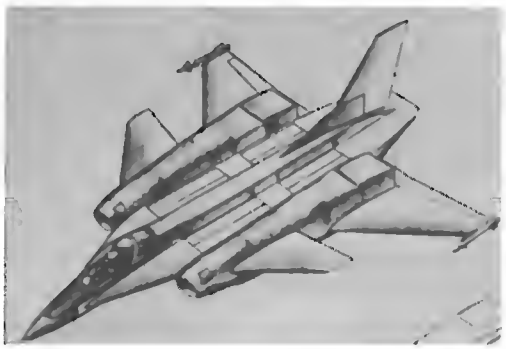

a) General Dynamics E-205 ejector

b) Grumman 623 RALS

c) Northrop HATOL (RALS)

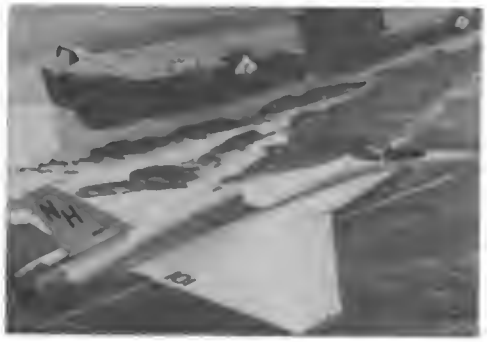

d) Northrop VATOL

e) Vought VATOL

Fig. 1: Twin-engine supersonic STOVL concepts

a) General Dynamics E-7 ejector

b) Rockwell ejector

c) McDonnell Douglas 279-3 vectored thrust

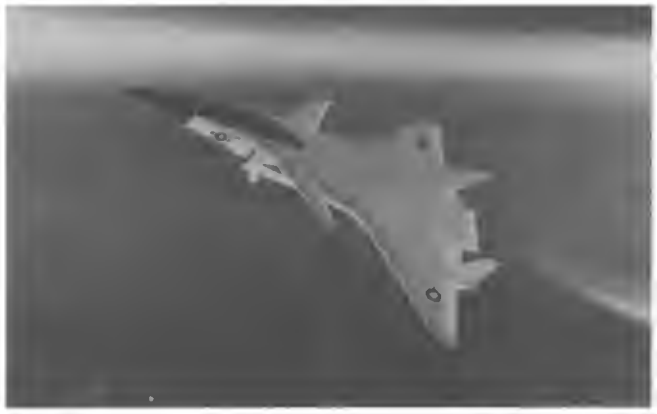

d) Vought TF-120 tandem fan

Fig. 2: Single-engine supersonic STOVL concepts

extensive, high-quality aerodynamic data base for modern STOVL fighter aircraft. The models and the wind tunnels in which they were tested are identified in Fig. 3. The models were tested over the entire Mach number range from post-transition flight (Mach = 0.2) to high supersonic speeds (Mach = 2 or greater). Reynolds number was held constant throughout the tests (usually at a value of 3×10^6/ft) except for limited excursions to determine the effect of this parameter. All experimental data for the STOVL fighter configurations presented in this paper are from the tests shown in Fig. 3 plus a jet-effects test of the 279-3 concept (discussed in the next section). The experimental results have been corrected for model base, cavity and internal drags, and for wall and buoyancy effects where applicable.

The following discussion will first cover aerodynamic highlights from the wind tunnel tests and predictions for several STOVL concepts, and then performance comparisons between STOVL and CTOL fighters will be presented.

STOVL AND CTOL AIRCRAFT AERODYNAMICS

AERODYNAMIC/PROPULSIVE INTERACTIONS FOR THE 279-3 VECTORED THRUST CONCEPT — A primary uncertainty about the 279-3 concept (Fig. 4a) is the supersonic drag because of the central location of the engine and the presence of the jet plumes in the vicinity of the aft fuselage. The overall airframe drag level was measured in the flow-through model tests mentioned above, but these tests did not provide any information about the jet plume effects. A powered test of the 279-3 was run using a jet-effects version of the wind tunnel model to measure these effects.

The jet-effects model is shown installed in the 9- by 7-Foot Supersonic Wind Tunnel in Fig. 4b. The most obvious difference between this model and the flow-through model in Fig. 3 is the mounting arrangement. The flow-through model was supported by a conventional rear-entry sting, which greatly distorts the aft fuselage contours. The jet-effects model was supported by a thin blade strut in the location of the vertical tail so as to leave the sides and bottom of the aft fuselage undistorted, permitting more accurate simulation of the flow around

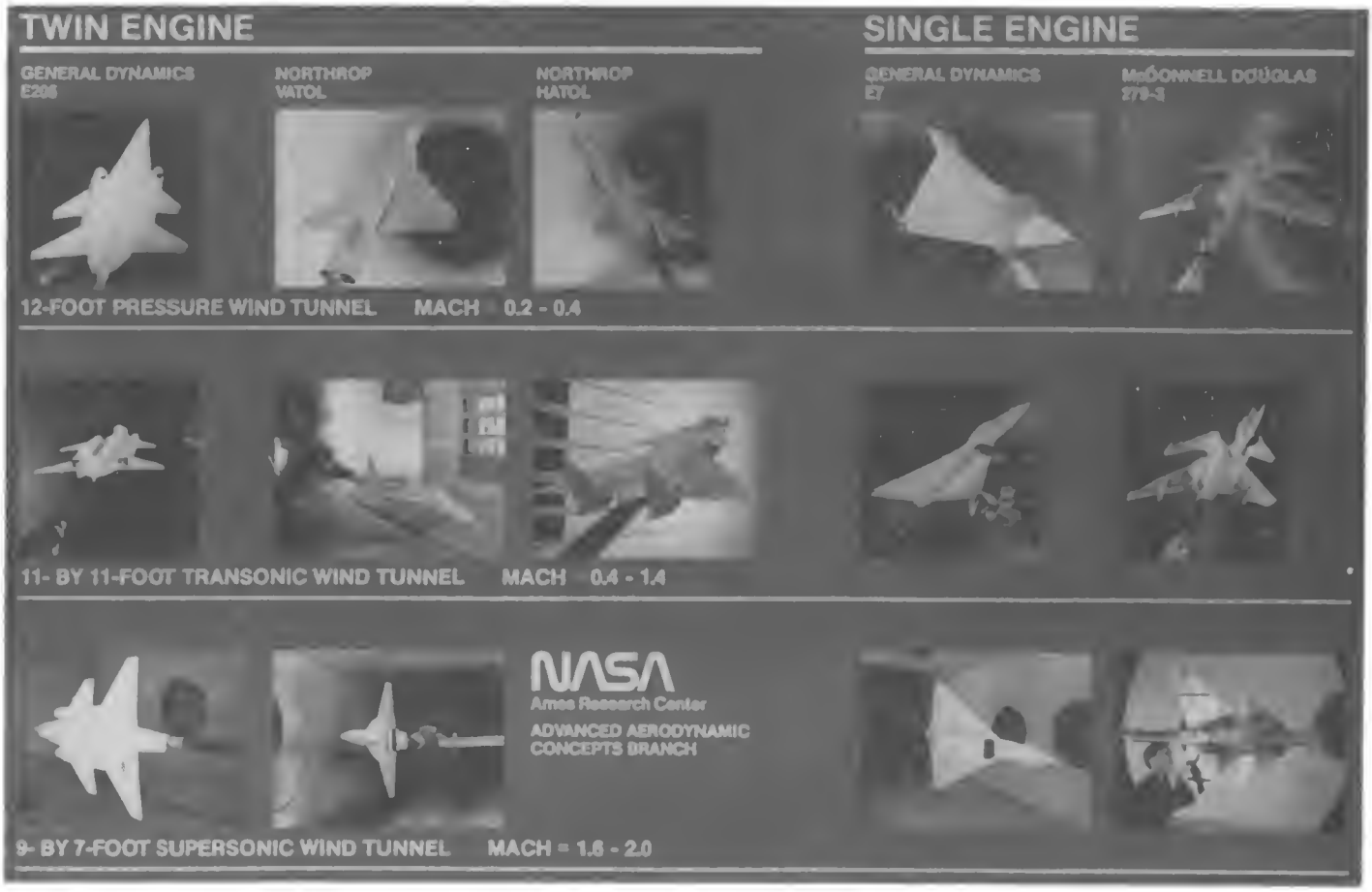

Fig. 3: Wind tunnel tests summary for the twin- and single-engine STOVL models

this part of the model. High-pressure (3000 psi) air was pumped into the model through the blade strut, where it was fed to the four nozzles via an internal plenum. The nozzles and high-pressure air hardware were non-metric (forces not measured by the balance), so that the balance measured only the airframe aerodynamics and the interaction of the jet plumes with the aerodynamics. The high-pressure air was heated to prevent icing during the expansion through the nozzles, but no attempt was made to simulate the high temperatures of the exhaust flows from a real engine. The inlets were faired over in the jet-effects test. Comparable runs between this test and the flow-through test were obtained to provide a basis for drag buildups using the two tests. Inlet fairings and the vertical tail were tested on and off in the flow-through model 9×7-Foot wind tunnel test to simulate the jet-effects configuration, and a simulated sting and shroud were tested on and off in the jet-effects test to simulate the flow-through model mounting arrangement.

Minimum drag — The effect of the jet plumes on the zero-lift drag of the jet-effects model is shown in Fig. 5. The drag scale is not shown for technology transfer reasons (the scales for all other dependent variables shown in this paper are omitted for the same reason). The zero-lift drag over the entire Mach number range for the flow-through model is included to give an indication of the scale. The drag of the jet-effects model with the jets off roughly corresponds to the flow-through model drag. That is, all of the increments for the differences between the models (described above) have been applied to the jet-effects data, with one exception: the mass flow through the model nozzles for the jet-effects data is zero, while the mass flow for the flow-through data is that resulting from the freestream air flowing through the inlets to the nozzles. However, there is almost no drag difference between zero and equivalent "flow-through" mass flows as measured on the jet-effects model, so the correlation of the curves for the two models is accurate.

Comparing the jets "on" and "off" curves reveals an apparently substantial drag difference at Mach 1.6, and about half of that difference at Mach 2.4. These drag differences are probably caused by the jet plumes scrubbing on the aft fuselage and the additional wave drag caused by the presence of the plumes next to the fuselage. These differences can be better appreciated though, when expressed in terms of the longitudinal aircraft performance.

Specific excess power — The performance parameter chosen to illustrate the jet plume effects is specific

a) Artist's concepts

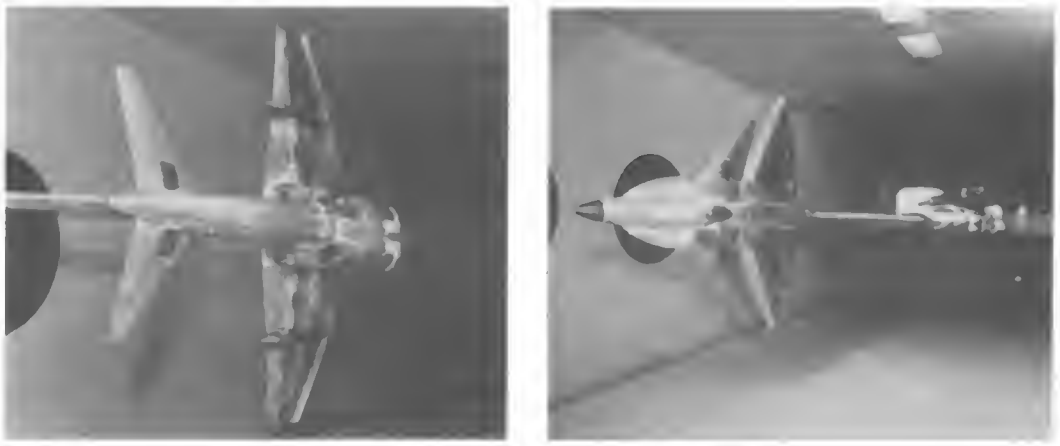

b) Jet effects model installed in 9- by 7-Foot Supersonic Wind Tunnel

Fig. 4: McDonnell Douglas 279-3 single-engine vectored thrust configuration

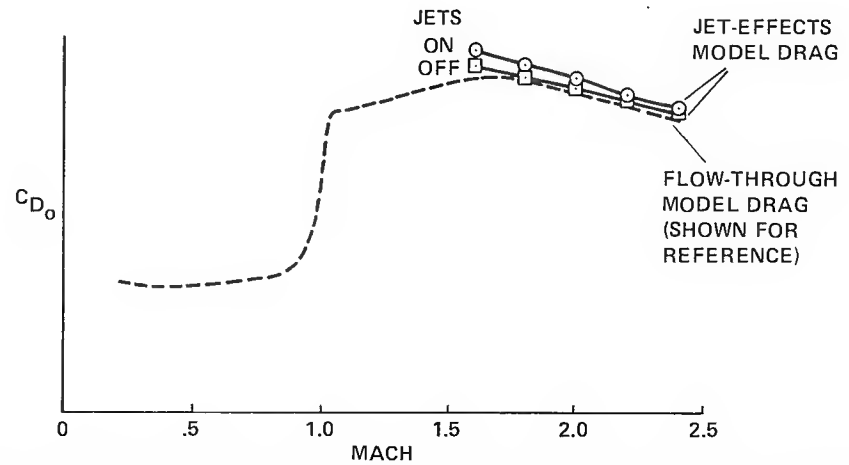

Fig. 5: Effect of propulsive/aerodynamic interactions on zero-lift drag for the 279-3 configuration

excess power, shown in Fig. 6 as a function of load factor. The wind tunnel drag data were adjusted to trimmed airplane conditions at an altitude of 30,000 ft for this plot. The contractor-estimated installed thrust was used in the calculation, and was held constant for the jets "on" and "off" curves to isolate the effects of the jet interactions with the airframe aerodynamics. The effect of the drag increase caused by the jets is a significant reduction in specific excess power at both Mach numbers. This verifies that the additional drag caused by the plumes in the proximity of the aft fuselage does significantly degrade the airplane performance, and ways to alleviate this problem would have to be seriously considered in any further developments of the 279-3 concept.

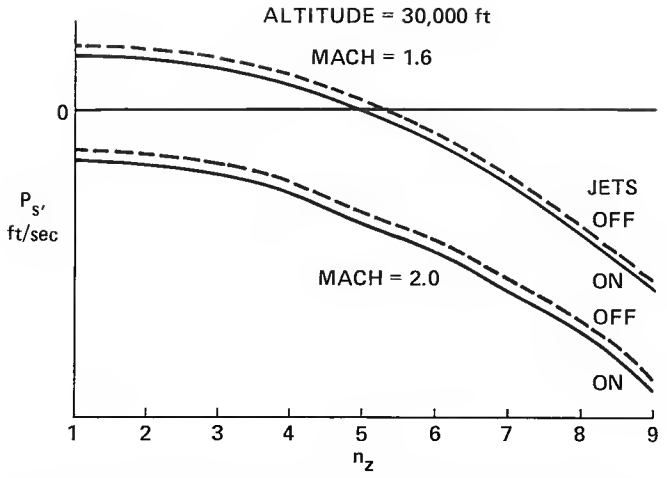

Fig. 6: Effect of propulsive/aerodynamic interactions on specific excess power for the 279-3 configuration

Plume visualization — Visualization of the plume locations relative to the airframe and of its areas of scrubbing on the aft fuselage can help identify some of the reasons for the drag increase caused by the jet plumes. Total pressure measurements within the plumes were acquired at three longitudinal fuselage stations by a 17-probe rake which was traversed vertically (relative to the model) behind the nozzles on the left side of the model. Static pressure measurements were acquired by 32 pressure taps on the left side of the aft fuselage. Shaded contour plots of these total and static pressure distributions are shown in Fig. 7 for a Mach number of 1.6 and an angle of attack of 10°. The nozzles were operating at their maximum power setting for the data in this figure. The lightest areas in the pressure plots indicate the presence of the plume, where the total pressure is high relative to freestream pressure and the static pressure is low. The fuselage cross sections are shown in the upper right of each of the total pressure plots, and the small "+" symbols represent the extended centerlines of the forward and aft nozzles at each fuselage station (the aft nozzle is above the forward nozzle). A side view of the aft fuselage geometry is shown in the static pressure plot, where the uppermost horizontal line represents the top of the fuselage in a true side view, the middle two horizontal lines bound the curved part of the lower aft fuselage, the lower of which having been "unwrapped" to the plane of the fuselage side (while maintaining constant arc length from the side), and the lowermost line represents the "unwrapped" bottom centerline of the fuselage. The aft nozzle exit plane and ramp are shown, as well as

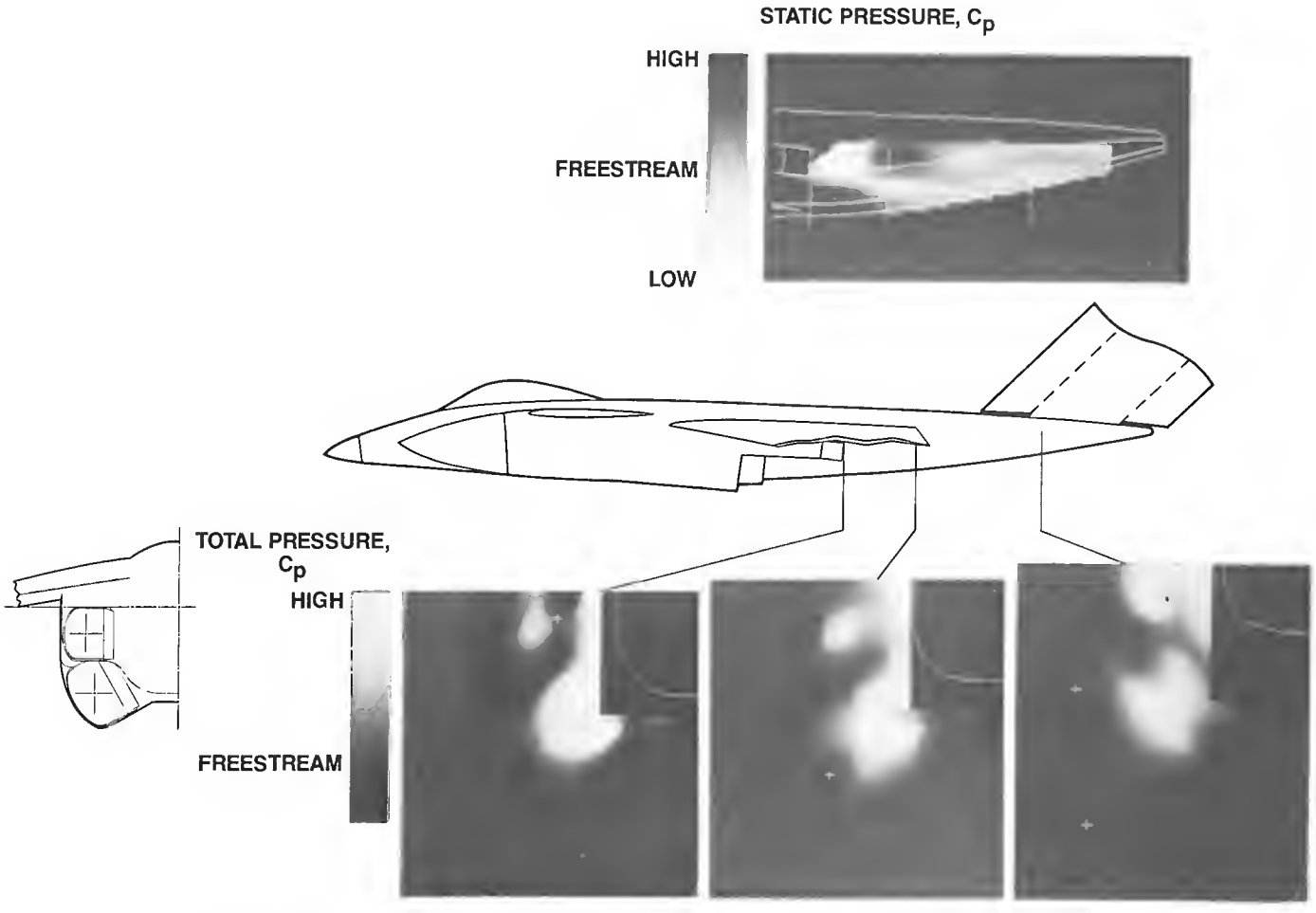

Fig. 7: Plume flow-field contours at Mach = 1.6, $\alpha = 10^{\circ}$, maximum power setting

a line extending from the forward nozzle lower lip (below the aft nozzle) to indicate the probable area of influence of the forward nozzle plume on the aft fuselage.

The total pressure distributions reveal that the aft nozzle plume is very close to the side of the fuselage at all three longitudinal stations, and is probably scrubbing on it at the two forward stations. The forward nozzle plume appears to be well away from the fuselage at all stations. Note that the plumes from both nozzles move upward and inboard relative to the extended nozzle centerlines as they flow downstream, which was an expected effect of the freestream flow. The static pressure distribution verifies the plume scrubbing on the fuselage, as shown by the lightest area of the plot immediately behind the aft nozzle. No scrubbing from the forward nozzle plume is evident in the area below the aft nozzle, but the possibility of scrubbing further upstream cannot be ruled out because the most-forward static pressure taps are well behind the forward nozzle exit.

The effects of the plume on the aft fuselage pressures can be isolated by comparing the pressures for the jets when on and off. Figure 8 shows the fuselage pressure distributions for power settings ranging from "off" to "maximum" for a Mach number of 1.6 and an angle of attack of 0°. Data in this figure are shown at a lower angle of attack than in the previous figure because the static pressures show the variation with power setting more clearly at the lower angle. The power "off" picture shows a mostly uniform distribution except for a small low-pressure area immediately behind the aft nozzle. This area is underneath the wing, and the low pressure here may be due to some aerodynamic separation or recirculation effect, since there is no flow out of the nozzles at this condition. Increasing the power to maximum levels shows a progression in the size of the region affected by the plume, verifying that the low pressure areas on the aft fuselage are the areas of plume impingement.

EVALUATION OF AERODYNAMIC PREDICTIONS — Selected aerodynamic predictions will be evaluated in this section for two of the subject STOVL fighter concepts. Only a small sample of prediction capabilities for high-speed STOVL fighter aircraft aerodynamics will be presented here, though it is recognized that a much more thorough coverage of this topic would be required to definitively summarize the state-of-the-art in these prediction capabilities. It should be noted that the predictions herein cover only the wing-borne flight modes of the aircraft, that is, no propulsive lift. Predictions of the longitudinal untrimmed aerodynamics will be discussed for the 279-3 and E-7 configurations.

McDonnell Douglas 279-3 vectored thrust configuration — A comparison of predicted and measured zero-lift and induced drag for the McDonnell Douglas (McAir) 279-3 configuration is shown in Fig. 9. The wind tunnel data are from the flow-through model tests since power effects were not included in the predictions, and the drag values have been adjusted to airplane conditions using the contractor's estimates for comparison with the airplane predicted drag.

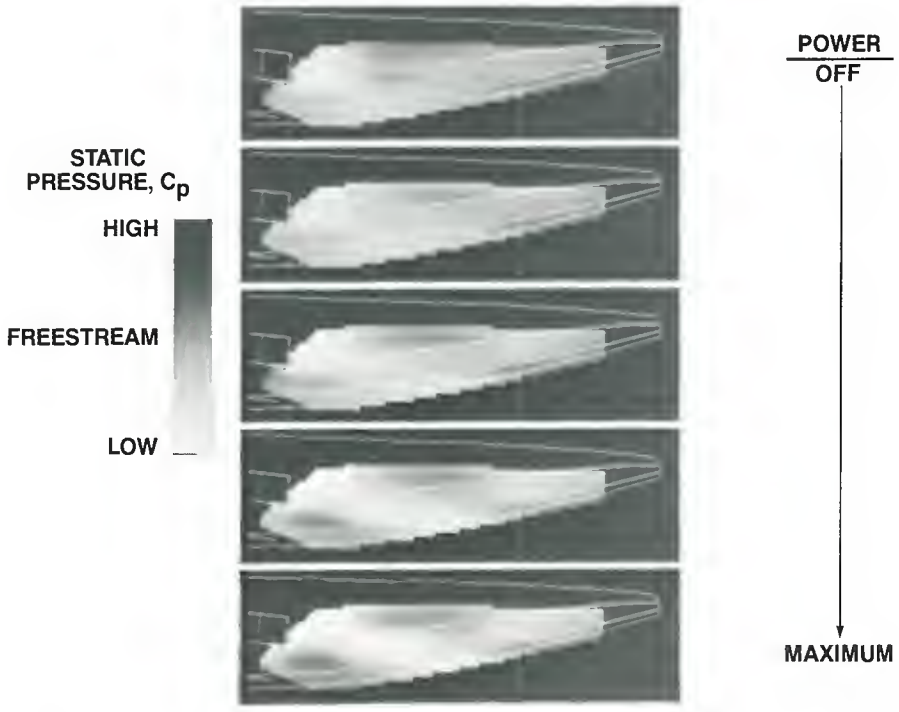

Fig. 8: Effect of nozzle pressure ratio on plume impingement at Mach = 1.6, $\alpha = 0°$

McAir used a combination of theoretical, analytical, and empirical methods to predict the zero-lift drag of their configuration. Among these methods were: the Karman-Schoenherr (turbulent) method (14) for predicting skin friction, the Sommer-Short T-Prime method (15) for compressibility effects, the NASA Langley Wave Drag Program (16) for wave drag, DATCOM (17) for transonic drag rise, and wind tunnel data from similar configurations to supplement all methods. Figure 9a shows that the low subsonic drag was predicted very well. However, the high subsonic drag prediction was too low before the rise and too high after the rise up to Mach 1. This is a difficult area in which to predict the drag, and the errors may be simply due to incorrect application of the method(s). It is significant that the total transonic drag increment is fairly close to the wind tunnel increment and the supersonic drag was predicted reasonably well, since the wave drag is a primary uncertainty for this configuration.

Induced drag measured in the wind tunnel at a Mach number of 0.2 is compared with that from three different prediction methods in Fig. 9b. The wind tunnel drag actually consists of more than just induced drag, since it was determined by subtracting the measured minimum drag from the total drag at all lift coefficients. The additional components of drag are primarily the form drag increases caused by boundary layer thickening and higher skin friction as lift is increased, but these are expected to be small relative to the actual induced drag. The McAir prediction method is again a combination of methods, such as the Langley vortex lattice code (18), the Woodward wing-tail-body code (19), a version of the Middleton-Carlson method (20), and McAir empirical methods with similar-

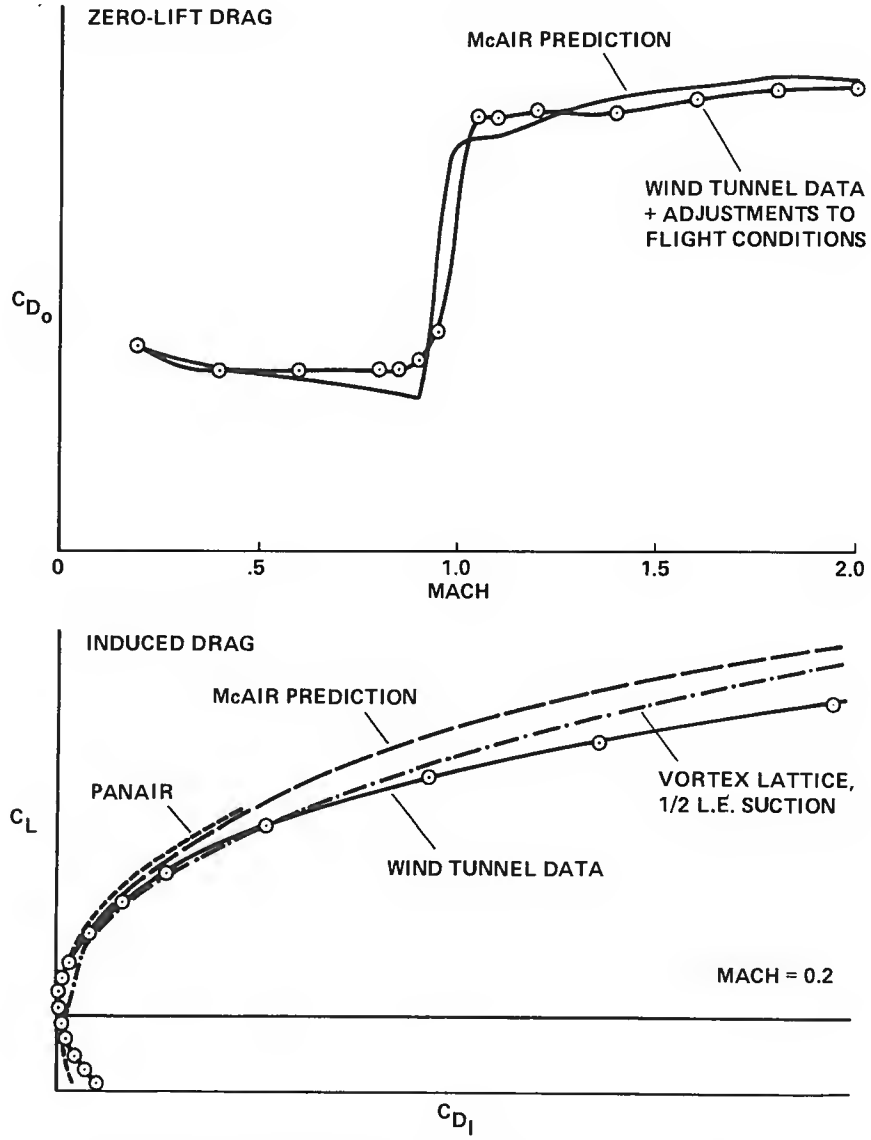

Fig. 9: Comparison of predicted and measured drag for the 279-3 configuration
a) Zero-lift drag, b) Induced drag

configuration wind-tunnel data. The figure shows that the McAir drag prediction was low over the entire range of lift coefficients. The PAN AIR (21) program is a linear potential code which does not contain vortex lift or viscous effects, so its underprediction of the induced drag is not surprising. The best induced-drag prediction is the curve identified as a vortex lattice method using one-half leading-edge ("1/2-L.E.") suction. This particular vortex lattice program was written at Stanford University and later modified to include the Polhamus suction analogy (22). The analogy was incorporated by rotating a user-specified percentage of an element axial force to the normal direction in order to approximate a vortex lift increment. It was found by iteration after the test data were acquired that converting 50% of the axial force to normal force yielded the best overall lift and drag prediction. The induced drag estimated by this vortex lattice method is very close to the wind tunnel data for the lower half of the range of lift coefficients plotted.

Lift and pitching-moment characteristics at Mach 0.2 from the wind tunnel data and from the three predictions previously discussed are shown in Fig. 10. As with the induced drag predictions, the vortex lattice method with the one-half leading-edge suction gave an excellent lift prediction at the lower angles of attack, but fell short of the test data at higher angles. Separated flow effects are not included in this method, so it did not predict the stall break in the lift curve. The vortex lattice pitching moment prediction was not as good as the lift or drag prediction, but could probably be improved by modeling the geometry more accurately with more vortex elements. The PAN AIR-predicted lift and pitching-moment curve slopes are very close to the slopes of the test data curves at low angles of attack, which is attributable to the arbitrary body modeling used in PAN AIR. Not surprisingly, the PAN AIR prediction does not follow the upward curvature of the measured lift curve at 10° angle of attack, so the prediction was not attempted above this angle. The McAir method overpredicted the lift at all angles of attack, but very closely estimated the maximum lift as measured in the wind tunnel. The prediction of the pitching moment curve slope in the low angle-of-attack range by the McAir method was close to that of the wind tunnel data, although it missed the zero-lift pitching moment and the initial break in the pitching moment curve. The direction of the break at maximum lift was correctly predicted.

General Dynamics E-7 ejector configuration — The E-7 aircraft concept and a wind-tunnel-model photograph are shown in Fig. 11. The one-ninth scale model is shown installed in the Ames 11- by 11-Foot Transonic Wind Tunnel. This configuration was derived from the F-16 fighter, and geometric similarities in the nose, inlet and vertical tail between the E-7 and the F-16 are easily recognized. Aside from the delta wing, obvious differences from the F-16 are the larger inlet size (needed for the higher mass flows required for vertical flight operations) and the much greater fuselage volume under the wing of the E-7. This large cross-sectional area around the engine location contributes to uncertainty about the wave drag and supersonic performance of the aircraft.

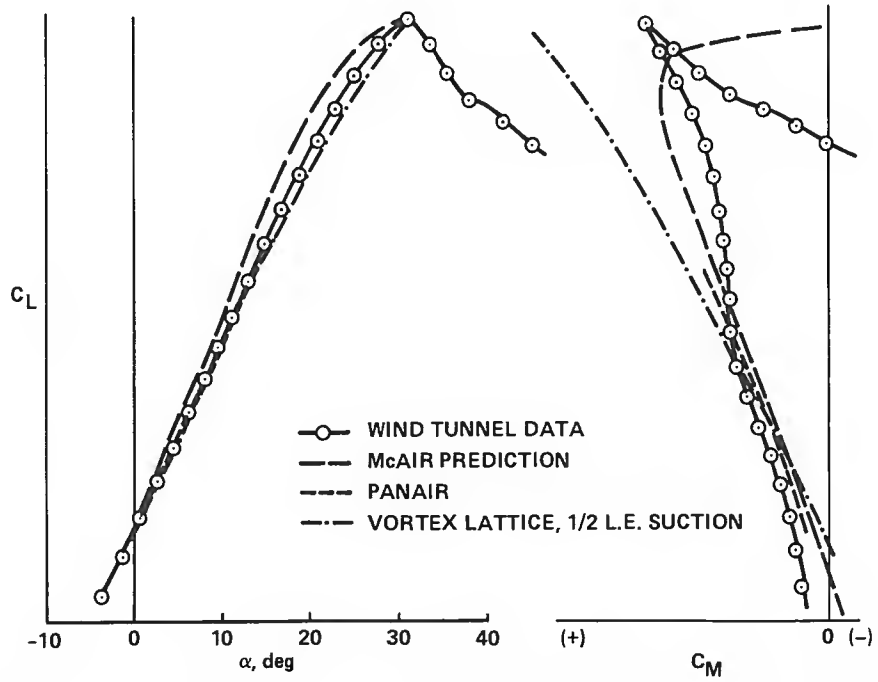

Fig. 10: Comparison of predicted and measured lift and pitching moment for the 279-3 configuration a) Lift; b) Pitching moment

a) Artist's concept

b) Model installed in 11- by 11-Foot Transonic Wind Tunnel

Fig. 11: General Dynamics E-7 single-engine ejector configuration

The measured and predicted zero-lift/zero-camber drag of the E-7 configuration are shown in Fig. 12. As with the 279-3 drag, the E-7 wind-tunnel-measured drag is untrimmed and has been adjusted to airplane conditions using the contractor's estimates. The subsonic drag prediction is excellent, and the wave drag prediction through the transonic range is also very close to the wind tunnel increment. The prediction is low in the supersonic range, but it increases at the higher Mach numbers and approaches the wind tunnel drag at Mach 2. This drag increase at the high Mach numbers is attributable to a singularity in the prediction method caused by the flow normal to the wing leading-edge (60° sweep) becoming sonic at Mach 2. It should be noted that the prediction shown is preliminary and is based on a far-field method using a body of revolution for the supersonic drag, not accounting for minor effects such as the inlet boundary layer diverter drag or other interference effects. The prediction could be improved by using an arbitrary body modeling with flow conditions solved for in the near field, and by accounting for configuration details and interference effects.

To summarize the prediction capabilities, zero-lift drag can be reasonably well predicted for complicated geometries, though less-than-desirable wave drag estimates may be obtained if the geometry is oversimplified. Induced drag predictions are best at low angles of attack where little or no separation occurs, but the lack of viscous and vortex flow effects render induced drag predictions less useful at higher angles of attack. The Polhamus suction analogy may improve the predictions if the presence of vortex lift is reasonably certain, such as for configurations with highly-swept, sharp leading-edge surfaces. However, the 279-3 has a moderately-swept wing with slightly-rounded leading edges, so experimental data were required to determine the degree of application of the suction analogy. Estimating the degree of vortex lift and the maximum lift remains a challenge in lift predictions. Pitching-moment predictions tend to be less accurate than lift or drag predictions since the distribution of lift as well as the total lift must be correct. Separation further complicates the prediction since the location and degree of separation determine the direction of the change in longitudinal stability.

VOLUME INTEGRATION / DRAG BUILDUP CHARACTERISTICS — The integration of the additional propulsion system hardware required to give a fighter aircraft STOVL capability often results in greater volume and a poorer volume distribution than for a comparable conventional fighter aircraft. However, it is possible to minimize the adverse impact of the additional hardware by utilizing area ruling techniques and designing the airframe around the propulsion system. This section discusses the integration of volume in STOVL fighter aircraft relative to minimizing overall drag. Three of the subject STOVL fighter concepts will be used to illustrate these effects: the Northrop HATOL and the General Dynamics E-205 and R-104.

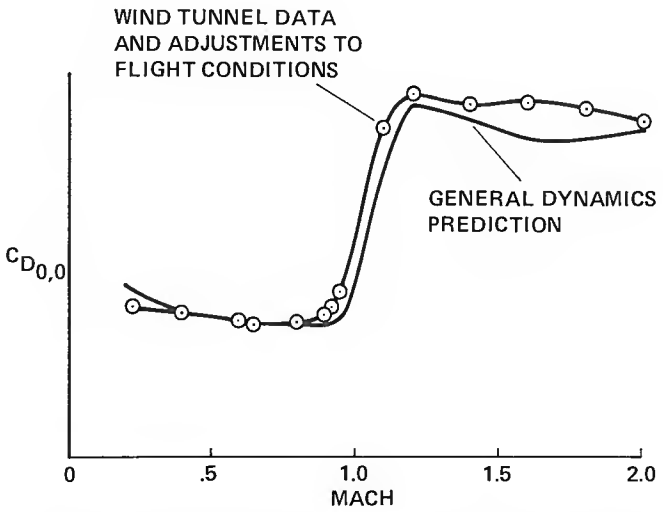

Fig. 12: Comparison of predicted and measured zero-lift/zero-camber drag for the E-7 configuration

Northrop HATOL configuration — An artist's concept drawing of the Northrop HATOL configuration and a photograph of the wind tunnel model installed in the 11- by 11-Foot Transonic Wind Tunnel are shown in Fig. 13. The HATOL is a twin-engine, canard-configured airplane, with twin vertical tails mounted on afterbody pods attached to the wing. Propulsive lift is provided by a remote augmentor lift system (RALS).

The ducting for the RALS in the fuselage occupies space that would normally be used for fuel, avionics, or other internal systems. Consequently, additional volume had to be created for these components. The afterbody pods holding the vertical tails provided a convenient volume in which to locate additional fuel and avionics, as well as the main landing gear. The drag increase caused by these pods would be of concern, however, not only because of the skin friction and form drag increments, but also the additional wave drag due to the shock interactions in the narrow channel between the pods and the fuselage side. Figure 14a shows a minimum drag component buildup for subsonic through supersonic Mach numbers from the HATOL wind tunnel tests. The lowermost curve in the plot represents the drag for the body and wing alone, BW, of the model. The other curves show the drag of the body and wing with the addition of the afterbody pods, BWP, the vertical tails on the pods, BWPV, and finally the canards, BWPVC, to complete the configuration. Comparing the two curves marked BW and BWP shows that the overall drag increment due to addition of the pods is almost negligible at Mach 1.1, while it is on the order of the canard and vertical tail increments at other Mach numbers. Considering that the frontal area of the pods is much greater than that of the canards or vertical tails, it is quite an achievement to integrate the pods with the rest of the airframe such that the minimum drag is similar to that of much thinner surfaces.

a) Artist's concept

b) Model installed in 11- by 11-Foot Transonic Wind Tunnel

Fig. 13: Northrop HATOL twin-engine RALS configuration

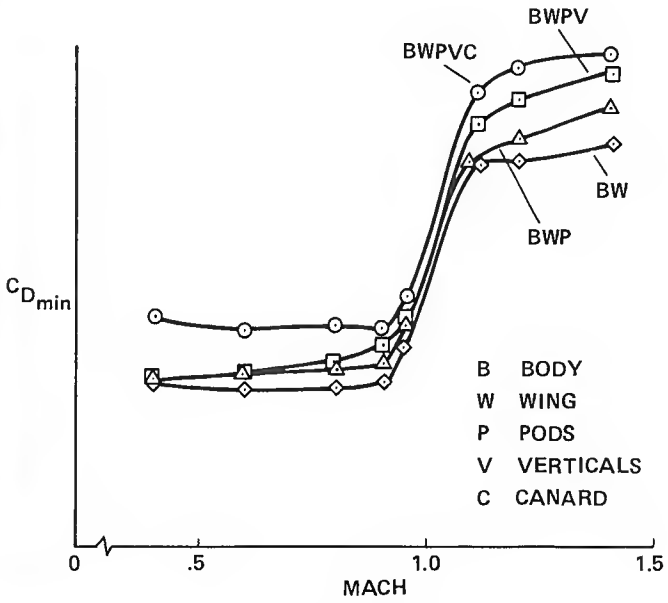

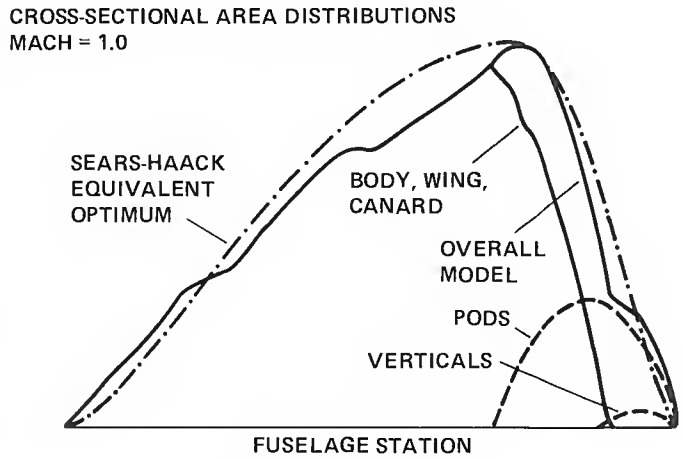

Fig. 14: Minimum drag component buildup for the HATOL configuration: a) Minimum drag; b) Cross-sectional area distributions, Mach = 1.0

One probable reason for the low drag increment of the pods can be seen in the Mach-1 normal area distributions for the HATOL model in Fig. 14b. The inlet stream-tube area and the fuselage distortion for the sting support have been removed from the model total area for this plot. The difference between the overall model and the body/wing/canard curves is the combined area of the pods and vertical tails. An area distribution for a Sears-Haack optimum body of revolution with the same volume, length, and location of maximum area as the complete HATOL model is included to illustrate a desired shape of the HATOL distribution. This plot shows that the addition of the pods and the vertical tails gives a more "filled-in" area distribution on the back side, which probably accounts for some reduction in the wave drag. To determine more specifically the effects of the pods on wave drag, more thorough correlations would have to be made between the test data and wave drag analysis program results along with consideration of the model normal and oblique area distributions.

General Dynamics E-205 ejector and R-104 RALS configurations — The two General Dynamics twin-engine configurations are derivatives of the Vectored-Engine-Over Wing (VEO-Wing) concept (23), which General Dynamics developed in a joint program with NASA and the Air Force. The goal of developing the ejector and RALS configurations was to study the feasibility of two different propulsion system concepts in similar airframes utilizing the VEO-Wing nozzles for enhanced maneuverability. The resulting E-205 and R-104 airplane concepts and photographs of the wind tunnel models are shown in Fig. 15. The concepts are similar except for the width and shape of the fuselages. The E-205 has widely spaced nacelles with the ejectors in between the nacelles and the center spine of the fuselage, forming two wide channels along the length of the fuselage (top and bottom) when the ejector doors are closed. The R-104 nacelles are closer together and the channel between the nacelles and the center spine is narrower than on the E-205. This narrower channel raises questions about possible higher wave drag relative to that of the E-205. A compromise in the design of the R-104 wind tunnel model could also contribute to higher wave drag, which would not be representative of the airplane characteristics. The spine of the fuselage immediately behind the canopy was made narrower than the rest of the spine further aft so that a common nose section could

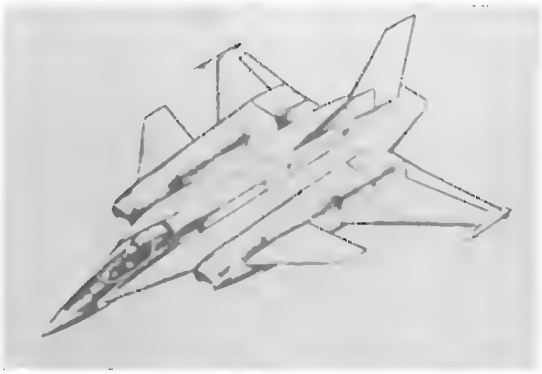

a) Artist's concept of E-205 ejector

b) Artist's concept of R-104 RALS

c) E-205 model installed in 12-Foot Pressure Wind Tunnel

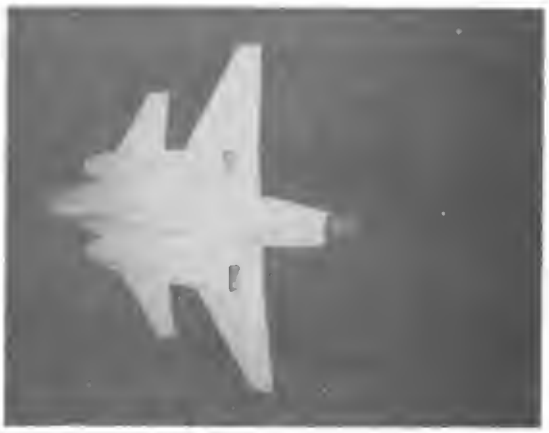

d) R-104 model installed in 9- by 7-Foot Supersonic Wind Tunnel

Fig. 15: General Dynamics twin-engine configurations

be used for both wind tunnel models. This results in a "necked-down" area on the model (Fig. 15d), which could cause separation and an increase in drag. Another difference between the two configurations is in the width of the aft body sections in the vicinity of the vertical tail. This section is much wider on the E-205 than on the R-104, which would certainly cause higher skin-friction drag, but the expected effects on the wave drag are uncertain.

The minimum drag characteristics of the two General Dynamics twin-engine models are shown in Fig. 16a over the full Mach-number range. The "body alone" curves reveal that the subsonic drag of both configurations is nearly equal, but the wave drag of the R-104 at the low supersonic Mach numbers is significantly higher. Adding the canard and wing to each configuration does not change the differences in drag between them, so any interference effects among the canard and wing and the fuselage/nacelle combination are the same for both configurations. The narrower channel and "necked-down" area behind the canopy of the R-104 are probably significant contributors to its higher drag. The cross-sectional area distributions of both configurations in Fig. 16b indicate that another probable contributor to the higher wave drag

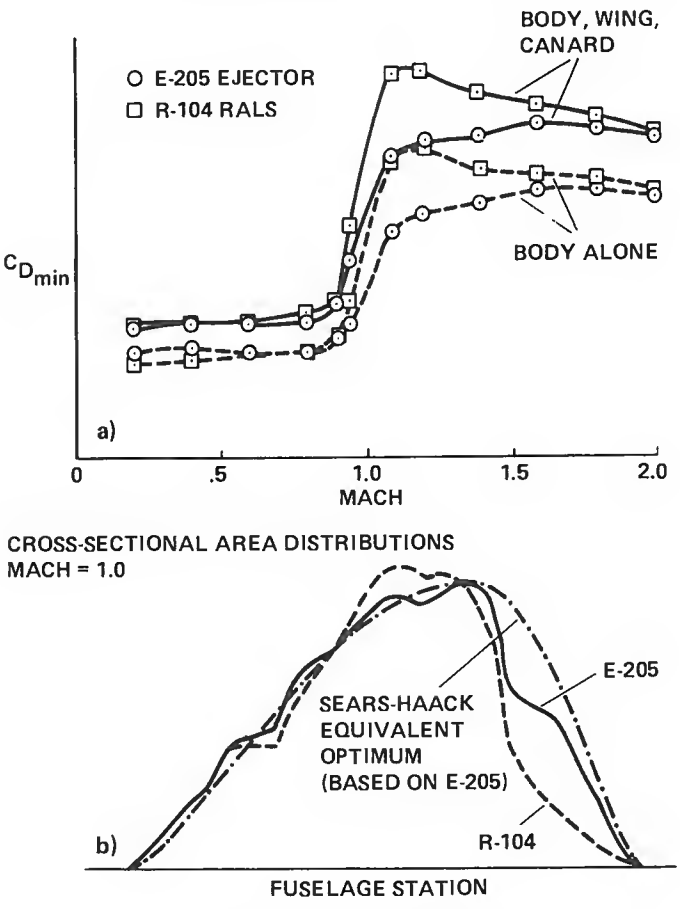

Fig. 16: Minimum drag component buildup for the General Dynamics twin-engine configurations
a) Minimum drag; b) Cross-sectional area distributions, Mach = 1.0

of the R-104 is a generally steeper slope on the back of the area distribution than for the E-205. This steeper slope is attributable to the narrower aft body of the R-104. The Sears-Haack optimum body area distribution based on the E-205 geometry shows that the E-205 distribution is closer to the desired shape, but it too could use some improvement. Even so, the greater volume in the aft fuselage of the E-205 and its resulting more-favorable area distribution, as a probable contributor to lower wave drag, supports the point made regarding the HATOL model that additional volume can be gained without excessive drag penalties if it is carefully tailored into the area distribution.

WAVE DRAG AND AERODYNAMIC EFFICIENCY COMPARISONS OF STOVL AND CTOL FIGHTERS — Attention will now be turned to comparisons of the performance of STOVL and conventional fighter aircraft in terms of wave drag and aerodynamic efficiency, expressed here as the maximum lift-to-drag ratio. Many more parameters would have to be considered in making a complete comparison of different aircraft, but these parameters are among the more critical ones for performance evaluation, and they will serve as indicators of the progress of aerodynamic technology development in the subject research program.

All of the STOVL aircraft data in this section are from the aforementioned wind tunnel tests, and have been trimmed and adjusted to airplane flight conditions as per the contractor's estimates of the wind-tunnel-to-flight adjustments. Data for the conventional aircraft are from the manufacturer's reports on flight-test results or wind-tunnel-test results adjusted to trimmed flight conditions.. The data shown are all that were available to the authors at the time of writing, so the reader should keep in mind that the results could be different if data from other aircraft were included. However, the present data are believed to be a reasonably representative sample of the total since a fairly broad range of aircraft geometrical characteristics are represented for both the STOVL and CTOL aircraft.

The aircraft associated with the conventional aircraft data points are not identified for technology transfer reasons. However, it can be said that all of the conventional aircraft represented herein are either in the current United States Air Force or Navy inventory, or have been retired from service within the past 15 years.

Wave drag — The first comparisons of STOVL and CTOL aircraft will be made in terms of the wave drag as a function of fineness ratio (Fig. 17a). For the purposes of this paper, the wave drag is defined as the increment in total drag between the Mach numbers of 0.8 and 1.2, and is based on the maximum cross-sectional area of each airplane. The comparison reveals that the wave drag of the STOVL aircraft on the whole is only slightly higher than that of the CTOL aircraft, while the fineness ratio of most of the STOVL aircraft is a little lower than

that of most of the CTOL aircraft. This observation is in contrast to what Alford and Harris (24) reported at a V/STOL aircraft conference over 20 years ago, which was that *all* of the V/STOL study concepts presented had lower fineness ratios and higher wave drag than *all* of the CTOL aircraft presented. The variation of wave drag with fineness ratio reported by Alford and Harris more clearly followed the theoretical wave drag variation shown in Fig. 17b than do the present data shown in Fig. 17a. These STOVL performance improvements are largely caused by increases in engine thrust-to-weight ratio and improvements in propulsion system installations, allowing more streamlined STOVL airframes.

Another way to evaluate wave drag trends for STOVL and CTOL aircraft is to consider the wave drag variation with location of maximum cross-sectional area (A_{MAX}). Figure 18 shows this variation for the same data as in Fig. 17a, along with a plot of the theoretical wave drag variation with location of A_{MAX}. The theoretical data were computed at a Mach number of 1.5 by the Harris Wave Drag Program (16) and a Lockheed version of the FLO57 Finite Volume Euler Program (from Jameson (25)). The programs indicate that the lowest wave drag is obtained when the maximum area is located about 50 to 60% along the length of the fuselage from the nose (the optimum location varies with Mach number). Note that the STOVL and CTOL aircraft data in Fig. 18a do not clearly follow the theoretical variations, but are more randomly scattered on the plot. However, this pattern is not too surprising since the only parameter held constant among all the data is A_{MAX}, while there are many other parameters or factors which affect wave drag. Some examples of these are fineness ratio, smoothness of the area distributions, protuberances, sweep, and aspect ratio. Thus, the relationship between wave drag and aircraft geometrical parameters is more complex than that predicted by simple theories. Perhaps a better way to make meaningful wave drag comparisons is by normalizing the data on more than just the reference area. Such further normalizations could lead to a better understanding of the characteristics that have the greatest effects on wave drag.

Aerodynamic efficiency -- A measure of the aerodynamic efficiency of an airplane in cruise flight is lift-to-drag ratio. This parameter can be correlated linearly with the ratio of the span of an aircraft to the square root of its wetted area for given values of the span efficiency factor and an effective skin-friction coefficient. (The effective

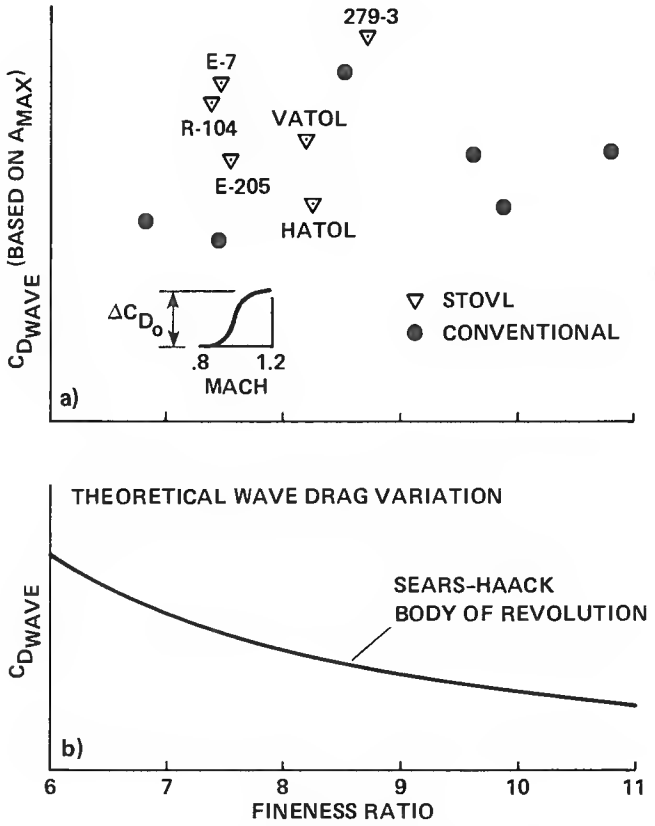

Fig. 17: Wave drag relative to fineness ratio for selected STOVL and conventional fighters: a) Measured results; b) Theoretical wave drag variation

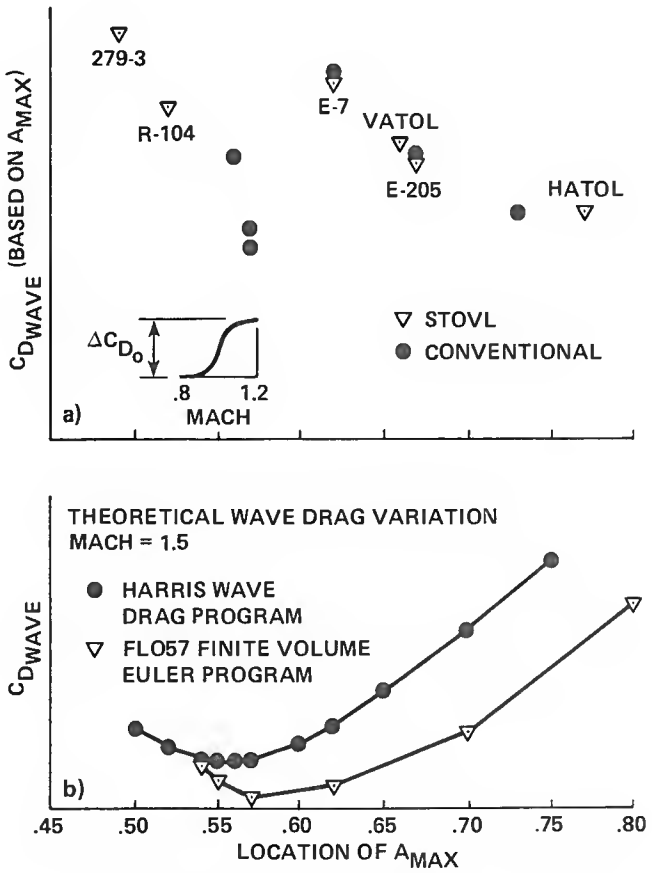

Fig. 18: Wave drag relative to location of maximum cross-sectional area for selected STOVL and conventional fighters: a) Measured results;
b) Theoretical wave drag variation, Mach = 1.5

skin-friction coefficient includes some form and pressure drag.) A comparison of the STOVL and CTOL aircraft of the previous two figures is shown in Fig. 19 at Mach numbers of 0.8 and 1.2 using this correlation. The equation for the correlation is given in the figure, and lines of constant values of the ratio of the effective skin friction to the span efficiency are shown.

At both Mach numbers, the STOVL aircraft have values of $(L/D)_{MAX}$ similar to those of the CTOL aircraft. The average value of $(b/\sqrt{S_{WET}})$ for the STOVL aircraft is slightly lower than that of the CTOL aircraft, but STOVL aircraft in general might be expected to have more wetted area because of the additional volume occupied by the propulsion system. Again this comparison of the types of aircraft shows progress relative to the results presented by Alford and Harris. In the earlier paper, the V/STOL aircraft were shown to have significantly lower aerodynamic efficiencies. The V/STOL data points in the other paper fell very closely along the same line of constant (C_f/e) as the CTOL aircraft, so the lower efficiencies were probably due primarily to higher wetted areas.

CONCLUSIONS

A high-speed aerodynamics research program has developed an extensive, high-quality aerodynamic database for a variety of twin- and single-engine supersonic V/STOL and STOVL fighter/attack aircraft. Many aerodynamic uncertainties associated with each aircraft concept have been resolved through the wind tunnel tests and analytical predictions performed in this program. Highlights of the results of this program have been presented, covering a broad range of areas of aircraft aerodynamics. These areas include jet plume/airframe interaction effects on drag and performance, longitudinal aerodynamic prediction capabilities for lift, drag, and pitching moment, integration of volume in the aircraft for drag minimization purposes, and wave drag and aerodynamic efficiency levels in comparison to conventional aircraft levels. Key conclusions drawn from each of these areas of discussion are:

1. Jet plume scrubbing on the aft fuselage of the 279-3 vectored thrust concept causes an increase in airframe drag and significantly degrades the specific excess power at supersonic Mach numbers.
2. Predicting zero-lift drag using a combination of analytical and empirical methods gives a reasonable preliminary estimate of the drag, but more refined methods using arbitrary geometries are required to obtain more reliable predictions.
3. Methods capable of predicting vortex and separated flows are required to estimate proper vortex lift increments and breaks in induced drag, lift, and pitching moment curves.

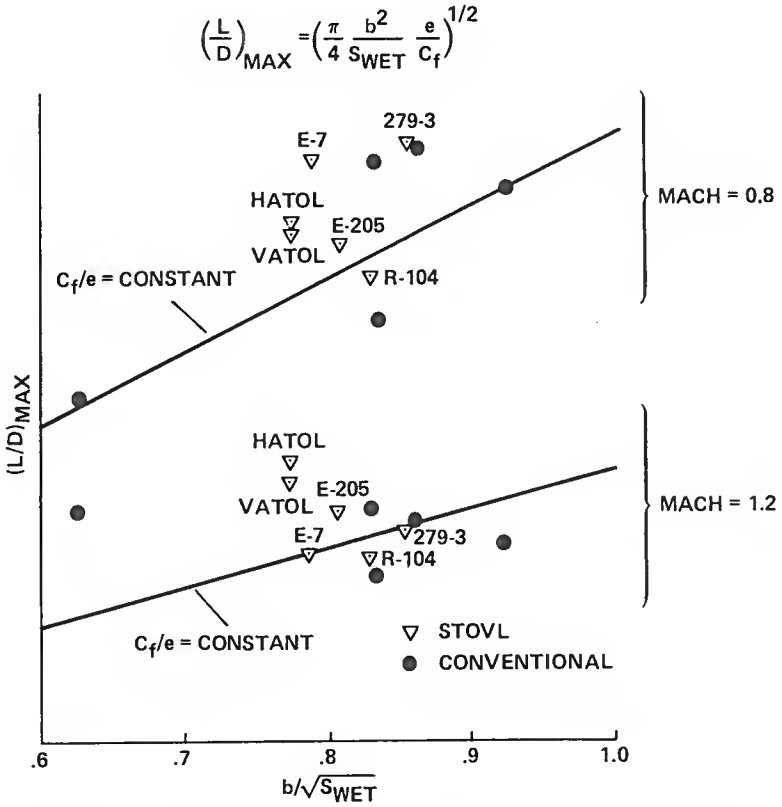

Fig. 19: Aerodynamic efficiency for selected STOVL and conventional fighters

4. Careful tailoring of an aircraft's cross-sectional area distribution by judicious placement of major components can alleviate volume-constraint problems in STOVL aircraft with minimal effect on overall drag.
5. STOVL fighter concepts appear to be comparable to CTOL fighters in wave drag and aerodynamic efficiency.
6. Simple theories do not adequately define the complex relationship between wave drag and aircraft geometric parameters.

REFERENCES

1. Anderson, S. B.: An Overview of V/STOL Aircraft Development. AIAA Paper 83-2491, October 1983.
2. Nelms, W. P.: Studies of Aerodynamic Technology for V/STOL Fighter/Attack Aircraft. AIAA Paper 78-1511, August 1978.
3. Nelms, W. P.; and Durston, D. A.: Preliminary Aerodynamic Characteristics of Several Advanced V/STOL Fighter/Attack Aircraft Concepts. SAE Paper 801178, October 1980.
4. Nelms, W. P.; Durston, D. A.: Concept Definition and Aerodynamic Technology Studies for Single Engine V/STOL Fighter/Attack Aircraft. AIAA Paper 81-2647, December 1981.
5. Lummus, J. R.: Study of Aerodynamic Technology for V/STOL Fighter/Attack Aircraft. NASA CR-152128, May 1978.
6. Foley, W. H.; Sheridan, A. E.; and Smith, C. W.: Study of Aerodynamic Technology for Single-Cruise-Engine V/STOL Fighter/Attack Aircraft. NASA CR-166268, February 1982.
7. Mark, Leon: Study of Aerodynamic Technology for Single-Cruise-Engine V/STOL Fighter/Attack Aircraft. NASA CR-166270, February 1982.
8. Burhans, Walter R. Jr.; Crafa, Vincent J., Jr.; Dannenhoffer, Nicholas F.; Dellamura, Frank A.; and Krepski, Robert E.: Study of Aerodynamic Technology for V/STOL Fighter/Attack Aircraft. NASA CR-152129, May 1978.
9. Brown, S. H.: Study of Aerodynamic Technology for V/STOL Fighter/Attack Aircraft. NASA CR-152130, May 1978.
10. Hess, J. R.; and Bear, R. L.: Study of Aerodynamic Technology for Single-Cruise-Engine V/STOL Fighter/Attack Aircraft. NASA CR-166269, February 1982.
11. Driggers, Herbert H.: Study of Aerodynamic Technology for Single-Cruise-Engine V/STOL Fighter/Attack Aircraft. NASA CR-166271, February 1982.
12. Gerhardt, H. A.; and Chen, W. S.: Study of Aerodynamic Technology for V/STOL Fighter/Attack Aircraft. NASA CR-152131, May 1978.
13. Driggers, Herbert H.: Study of Aerodynamic Technology for V/STOL Fighter/Attack Aircraft. NASA CR-152132, May 1978.
14. Schoenherr, K. E.: Resistance of Flat Surfaces Moving Through a Fluid. Transactions of the Society of Naval Architects and Marine Engineers, no. 40, p. 279, 1932.
15. Sommer, S. C.; and Short, B. J.: Free-Flight Measurements of Turbulent Boundary Layer Skin Friction in the Presence of Severe Aerodynamic Heating at Mach Numbers from 2.8 to 7.0. NACA TN-3391. March 1955.
16. Harris, R. V.: An Analysis and Correlation of Aircraft Wave Drag. NASA TM X-947. March 1964.
17. Hoak, D. E.: USAF Stability and Control DATCOM. USAF WADD TR-60-261, April 1978 edition.
18. Margason, R. J.; and Lamar, J. E.: Vortex-Lattice Fortran Program for Estimating Subsonic Aerodynamic Characteristics of Complex Planforms. NASA TN-D-6142, February 1971.
19. Woodward, F. A.; and Hague, D. S.: A Computer Program for the Analysis and Design of Wing-Tail-Body Combinations at Subsonic and Supersonic Speeds. ARC-TN-19, March 1969.
20. Shrout, Barrett L.: Extension of a Numerical Solution for the Aerodynamic Characteristics of a Wing to Include a Canard or Horizontal Tail. NASA TM X-66886, January 1971.
21. Magnus, Alfred E.; and Epton, Michael E.: PAN AIR - A Computer Program for Predicting Subsonic or Supersonic Linear Potential Flows About Arbitrary Configurations Using a Higher Order Panel Method, vol. I - Theory Document (Version 1.0). NASA CR-3251, April 1980.
22. Polhamus, Edward C.: A Concept of the Vortex Lift of Sharp-Edge Delta Wings Based on a Leading-Edge Suction Analogy. NASA TN D-3767, December 1966.
23. Woodrey, R. W.: An Experimental Investigation of a Vectored-Engine-Over-Wing Powered-Lift Concept. AFFDL-TR-76-92, Volumes I and II, September 1976.
24. Alford, William J., Jr.; and Harris, Roy V.: Cruise Performance and Stability Considerations for Jet V/STOL Aircraft. Paper no. 11, NASA SP-116, April 1966.
25. Jameson, A.; Schmidt, W.; and Turkel, E.: Numerical Solutions of the Euler Equations by Finite Volume Methods Using Runge-Kutta Time-Stepping Schemes. AIAA Paper 81-1259, June 1981.

NASA
National Aeronautics and Space Administration

Report Documentation Page

1. Report No.	2. Government Accession No.	3. Recipient's Catalog No.
NASA TM-100061		

4. Title and Subtitle	5. Report Date
Wave Drag and High-Speed Performance of Supersonic STOVL Fighter Configurations	January 1988
	6. Performing Organization Code

7. Author(s)	8. Performing Organization Report No.
Donald A. Durston and Ronald K. Stonum	A-88072
	10. Work Unit No. 505-61-71

9. Performing Organization Name and Address	11. Contract or Grant No.
Ames Research Center Moffett Field, CA 94035	
	13. Type of Report and Period Covered
12. Sponsoring Agency Name and Address	Technical Memorandum
National Aeronautics and Space Administration Washington, DC 20546-0001	14. Sponsoring Agency Code

15. Supplementary Notes

Point of Contact: Donald A. Durston, Ames Research Center, MS 227- 2 Moffett Field, CA 94035
(415) 694-6216 or FTS 464-6216
Presented at International Powered Lift Conference in Santa Clara, CA, Dec. 7 - 10, 1987

16. Abstract

A supersonic STOVL fighter aircraft aerodynamic research program is being conducted at NASA Ames Research Center. The research focuses on technology development for this type of aircraft and includes generating an extensive aerodynamic database and resolving particular aerodynamic uncertainties for various twin- and single-engine aircraft concepts. Highlights of the results from this program are presented. The highlights include propulsion-induced effects on the aircraft drag, prediction capabilities, volume integration for minimizing drag, and wave drag and aerodynamic efficiency comparisons. Results indicate that estimated STOVL fighter performance is roughly comparable to the performance of modern conventional fighters in terms of wave drag and aerodynamic efficiency.

17. Key Words (Suggested by Author(s))	18. Distribution Statement
VSTOL STOVL fighters Aerodynamics Aerodynamic efficiency Wave drag	Unclassified-Unlimited Subject Category – 02

19. Security Classif. (of this report)	20. Security Classif. (of this page)	21. No. of pages	22. Price
Unclassified	Unclassified	18	A02